Perfectly matched layers for Maxwell's equations in second order formulation

Björn Sjögreen
N. Anders Petersson

U.S. Department of Energy

Lawrence
Livermore
National
Laboratory

July 26, 2004

DISCLAIMER

Perfectly matched layers for Maxwell's equations in second order formulation[*]

Björn Sjögreen[†]   N. Anders Petersson[‡]

July 26, 2004

Abstract

We consider the two-dimensional Maxwell's equations in domains external to perfectly conducting objects of complex shape. The equations are discretized using a node-centered finite-difference scheme on a Cartesian grid and the boundary condition are discretized to second order accuracy employing an embedded technique which does *not* suffer from a "small-cell" time-step restriction in the explicit time-integration method. The computational domain is truncated by a perfectly matched layer (PML). We derive estimates for both the error due to reflections at the outer boundary of the PML, and due to discretizing the continuous PML equations. Using these estimates, we show how the parameters of the PML can be chosen to make the discrete solution of the PML equations converge to the solution of Maxwell's equations on the unbounded domain, as the grid size goes to zero. Several numerical examples are given.

1   Introduction

In this paper, we study grid convergence properties of numerical solutions of the two-dimensional Maxwell's equations, when a perfectly matched layer (PML) is used to truncate an unbounded domain. While there are many types of non-reflecting and absorbing boundary conditions, we here choose to use PML because it is a simple and straightforward method, easily implemented for both two and three space dimensions using either

---

[†]Royal Institute of Technology, 100 44 Stockholm, Sweden, `bjorns@nada.kth.se`

[‡]Center for Applied Scientific Computing, Lawrence Livermore National Lab, Livermore, CA 94551, `andersp@llnl.gov`.

1

Cartesian or cylindrical/spherical coordinates. The PML technique, which first was proposed by Berenger [5], is based on modifying the partial differential equation (PDE) away from all physical boundaries such that

a) waves of all frequencies and angles are transmitted from the interior into the layer without any reflections, and

b) the PML damps waves so that they become insignificant before they reach the outer boundary of the computational domain.

The PML equations are derived by Fourier transforming in time and modifying the Fourier-transformed problem to satisfy conditions a) and b). New dependent variables are introduced to allow the modified equations to be transformed back to the time variable. Waves at all angles and frequencies are damped by the PML, but the damping depends on the angle between the impinging wave and the PML interface, and goes to zero for glancing waves. When the PML is truncated to a finite width, the exponentially small remainder of the waves is reflected at the outer boundary.

To illustrate the basic ideas, we consider the Cauchy problem for the one-dimensional version of the TM_z equations,

$$\frac{\partial \mathcal{H}^{(y)}}{\partial t} = \frac{\partial \mathcal{E}^{(z)}}{\partial x}, \quad -\infty < x < \infty, \tag{1}$$

$$\frac{\partial^2 \mathcal{E}^{(z)}}{\partial t^2} = \frac{\partial^2 \mathcal{E}^{(z)}}{\partial x^2}, \quad -\infty < x < \infty. \tag{2}$$

We are interested in computing the solution in the half-plane $x < 0$ and introduce a PML in $x > 0$. In all practical computations, the thickness of the PML must be limited and we here truncate the PML at $x = d > 0$, where a homogeneous Dirichlet condition is imposed. The one-dimensional PML equations are

$$\frac{\partial H^{(y)}}{\partial t} = \frac{\partial E^{(z)}}{\partial x} - \sigma(x)H^{(y)},$$

$$\frac{\partial^2 E^{(z)}}{\partial t^2} = \frac{\partial^2 E^{(z)}}{\partial x^2} - \sigma(x)\frac{\partial E^{(z)}}{\partial t} - \frac{\partial}{\partial x}\left(\sigma(x)H^{(y)}\right), \quad -\infty < x < d, \tag{3}$$

$$E^{(z)}(d, t) = 0,$$

where the coefficient of the damping term satisfies

$$\sigma(x) = \begin{cases} 0, & x < 0, \\ \sigma_{max}P(x), & 0 \leq x \leq d, \end{cases}$$

for some non-negative function $P(x) \leq 1$. Here, $\sigma_{max} > 0$ is a constant. Note that we distinguish between Maxwell's equations and the PML equations by using calligraphic

letters for the solution of the former problem. The system (1)-(2) has traveling-wave solutions propagating to the right (increasing x) given by (for simplicity we only consider the $\mathcal{E}^{(z)}$-component)

$$\mathcal{E}^{(z)}(x,t) = Ae^{i\omega(t-x)},$$

and the corresponding solution of the PML equations is

$$E^{(z)}(x,t) = A\left(-e^{i\omega(t+x-2d)+\int_0^x \sigma(s)\,ds - 2\int_0^d \sigma(s)\,ds} + e^{i\omega(t-x)-\int_0^x \sigma(s)\,ds}\right).$$

Outside the PML ($x < 0$), the difference between the solutions is an exponentially small wave traveling to the left,

$$e_1(x,t) =: \mathcal{E}^{(z)}(x,t) - E^{(z)}(x,t) = Ae^{i\omega(t+x-2d)-2\int_0^d \sigma(s)\,ds}.$$

We call e_1 the PML modeling error. This expression illustrates the well-known result that the error due to solving the PML equations on a truncated computational domain is determined by the integral of $\sigma(x)$. In two space dimensions, the angle between the impinging wave and the PML modifies the expression, but the basic conclusion still holds.

To solve the continuous PML equations numerically, we discretize the problem and this process introduces a discretization error. In the present paper we want to study how to choose $\sigma(x)$ so that both the PML modeling error and the discretization error converge to zero as the grid size $h \to 0$. The PML modeling error is the same for all functions $\sigma(x)$ with the same value of $\int_0^d \sigma(s)\,ds$, but the discretization error is more sensitive to the particular choice of $\sigma(x)$. For a second order accurate staggered discretization of the one-dimensional model problem, we show that the discretization error satisfies

$$e_2 \le Ch^2(1 + \sigma_{max}^3)e^{c_2 t},$$

when the function $P(x)$ and its two first derivatives are bounded independently of h. To make the PML modeling error go to zero as $\mathcal{O}(h^2)$ when $h \to 0$, σ_{max} must increase as $|\log h|$, if the thickness of the PML is constant. Thus, the total error $e_1 + e_2$ will go to zero as $\mathcal{O}(h^2|\log h|)$.

In two space dimensions, we consider the scattering problem where incoming waves are deflected by perfectly conducting objects of complex shape, see Figure 1. Maxwell's equations are discretized as a second order PDE instead of first rewriting it as a first order system, and then applying the commonly used staggered discretization. Discretizing the second order PDE allows us to use a node-centered finite-difference scheme on a Cartesian grid. The boundaries of the perfectly conducting objects are allowed to cut through the grid in an arbitrary fashion and we use the technique developed by Kreiss, Petersson and Yström [13, 14, 15] to discretize the boundary conditions to second order accuracy without imposing any "small-cell" time-step restrictions in the explicit time integration method. Inside the PML, we keep the second order formulation of the primary dependent variable, but use a first order formulation for the auxiliary PML variables.
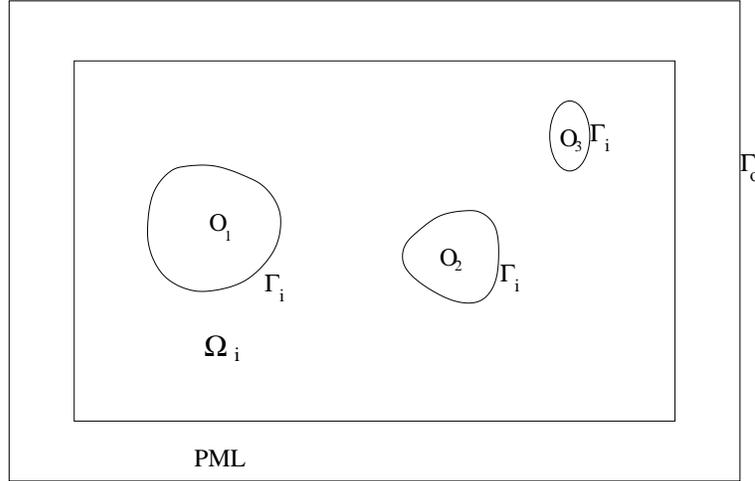
3

Figure 1: Sample domain outside three objects.

Thanks to the large number of publications triggered by Berenger's [5] original work on PML for Maxwell's equations, the properties of the continuous PML equations are by now well understood. However, there are significantly fewer investigations of the properties of numerical approximations of the PML equations. Most research is related to the Yee scheme of FDTD. Wu and Fang [19] considers a discontinuous $\sigma(x)$ which jumps between zero outside the PML and a positive value inside the PML. That paper suggests a modification of the σ-value right at the interface to minimize numerical reflection. Juntunen, Kantartzis and Tsiboukis [11] minimize numerical reflections with respect to the values of σ at the grid points inside the PML, but the PML has a fixed number of grid points. Asvadurov et al. [3] determines the discrete values of σ at the grid points from an optimization problem, making the values as close as possible to the pseudo-differential operator representation in Engquist and Majda [8]. The grid is non-uniform, but grid convergence is not considered. Some analysis of numerical reflection properties is also performed in Petropoulos [17].

In most previous work, σ is selected to be optimal on a given grid. One exception is the paper by Driscoll and Fornberg [7], where a scheme for Maxwell's equations with discontinuous coefficients is developed and some grid convergence studies are presented. However, they do not consider solving the equations on an unbounded domain, so they do not attempt to minimize the PML modeling error.

The original equations proposed by Berenger turned out to only be weakly hyperbolic which means that lower order terms can make the problem ill-posed and allow solutions that grow exponentially in time. But with the modifications introduced in the so called UPML equations, a strongly hyperbolic system was obtained that retained the non-reflective properties of the original PML equations [18]. A remaining minor difficulty with the UPML equations is that the zeroth order term can lead to algebraic growth in

time, due to a Jordan block in the matrix operating on that term. However, this growth can be avoided if the initial data are chosen to not excite that component of the solution, see Abarbanel, Gottlieb and Hesthaven [1] for a discussion. We will henceforth refer to the UPML equations as the PML equations.

There are many other types of non-reflecting boundary conditions for the wave equation and for Maxwell's equations. The most common approach is to use an exact formula for the far-field solution. In order to obtain a local (in time and space) boundary condition, some kind of approximation of the exact solution operator is introduced. Examples include the Padé technique by Engquist and Majda [8] as well as approximations of an integral kernel, see Alpert, Greengard and Hagstrom [2]. In the approach developed by Higdon [10], perfect transmission of outgoing waves can be guaranteed for a finite number of specified angles, and the accuracy of the approximation improves as more and more angles are taken into account. A variation of this technique is also used by Givoli and Neta [9].

The remainder of the paper is organized as follows. In Section 2 we derive the PML equations for the TM$_z$ mode of Maxwell's equations, both for Cartesian and cylindrical coordinates. The PML equations are discretized in Section 3, where also the embedded treatment of complex boundaries is described. Modeling and discretization errors in the PML approach are discussed in Section 4, and numerical experiments are presented in Section 5. Some conclusions and an outline of future work is given in Section 6.

2 Maxwell's equations with PML

We consider the TM$_z$ problem for Maxwell's equations, i.e., the two-dimensional case where the magnetic field lies in the (x, y)-plane, $\boldsymbol{H} = \mathcal{H}^{(x)}(x, y, t)\boldsymbol{e}_x + \mathcal{H}^{(y)}(x, y, t)\boldsymbol{e}_y$, and the electric field only has a component perpendicular to that plane, $\boldsymbol{E} = \mathcal{E}^{(z)}(x, y, t)\boldsymbol{e}_z$. By scaling the dependent variables and time, Maxwell's equations describing a homogeneous, lossless material without charges simplify to, cf. [4],

$$\frac{\partial \mathcal{H}^{(x)}}{\partial t} = -\frac{\partial \mathcal{E}^{(z)}}{\partial y}, \tag{4}$$

$$\frac{\partial \mathcal{H}^{(y)}}{\partial t} = \frac{\partial \mathcal{E}^{(z)}}{\partial x}, \qquad \text{in } \Omega, \quad t \geq 0, \tag{5}$$

$$\frac{\partial \mathcal{E}^{(z)}}{\partial t} = \frac{\partial \mathcal{H}^{(y)}}{\partial x} - \frac{\partial \mathcal{H}^{(x)}}{\partial y}, \tag{6}$$

subject to the constraint

$$\frac{\partial \mathcal{H}^{(x)}}{\partial x} + \frac{\partial \mathcal{H}^{(y)}}{\partial y} = 0, \quad \text{in } \Omega, \quad t \geq 0. \tag{7}$$

5

By cross-differentiation,

$$\frac{\partial^2 \mathcal{E}^{(z)}}{\partial t^2} = \Delta \mathcal{E}^{(z)}, \quad \text{in } \Omega, \quad t \geq 0, \tag{8}$$

where $\Delta = \partial^2/\partial x^2 + \partial^2/\partial y^2$. Initial data is given by

$$\mathcal{E}^{(z)}(x,y,0) = f(x,y), \quad \frac{\partial \mathcal{E}^{(z)}}{\partial t}(x,y,0) = g(x,y) =: \frac{\partial \mathcal{H}^{(y)}}{\partial x}(x,y,0) - \frac{\partial \mathcal{H}^{(x)}}{\partial y}(x,y,0).$$

We are interested in the case where the domain Ω is external to perfectly electric conducting (PEC) objects, see Figure 1. The boundary of the PEC objects will be denoted Γ_i. The PEC boundary condition $\boldsymbol{n} \times \boldsymbol{E} = 0$, where $\boldsymbol{n} = n^{(x)} \boldsymbol{e}_x + n^{(y)} \boldsymbol{e}_y$ is the outward normal of the boundary, becomes

$$\left(\boldsymbol{e}_x n^{(y)} - \boldsymbol{e}_y n^{(x)} \right) \mathcal{E}^{(z)} = 0, \quad \text{on } \Gamma_i,$$

i.e.,

$$\mathcal{E}^{(z)} = 0, \quad \text{on } \Gamma_i.$$

We solve the second order wave equation (8) for $\mathcal{E}^{(z)}$. The magnetic field can then be integrated passively because once $\mathcal{E}^{(z)}$ is known, equations (4)-(5) reduce to ordinary differential equations at each point of Ω.

The solution of the original problem (posed on the unbounded domain Ω) is computed inside a bounded sub-domain Ω_i. The PML is added outside of Ω_i, and the union of Ω_i and the PML layer defines the computational domain Ω_c. In Figure 1, we display an example of Ω_i with three objects, (O_1, O_2, and O_3), surrounded by a PML. The outer boundary of the PML will be denoted Γ_o.

Basic properties and derivation of a PML can be found in [18]. Here, we only give a brief introduction to the underlying ideas. We begin by Fourier transforming the solution of the wave equation (8) in time,

$$\mathcal{E}^{(z)}(x,y,t) = \frac{1}{\sqrt{2\pi}} \int_{-\infty}^{\infty} \widehat{\mathcal{E}^{(z)}}(x,y,\omega) e^{i\omega t} \, d\omega.$$

In the absence of boundaries, the wave equation has plane wave solutions,

$$\widehat{\mathcal{E}^{(z)}}(x,y,\omega) = e^{-i\omega(k_1 x + k_2 y)}.$$

Here k_1 and k_2 are real and normalized to satisfy $k_1^2 + k_2^2 = 1$. In this way, the vector (k_1, k_2) becomes the unit direction of the wave. Let us consider the case where we want to compute the solution in the quarter-plane $x < x_0$, $y < y_0$. The PML is introduced outside that quarter plane, that is, in $x > x_0$ and $y > y_0$. Let us look for a modification of the wave equation such that it gets exponentially decaying solutions in the PML,

$$\widehat{E^{(z)}}(x,y,\omega) = e^{-k_1 S_1(x) - k_2 S_2(y)} e^{-i\omega(k_1 x + k_2 y)}. \tag{9}$$

Here $S_1(x)$ is a real-valued function which is zero for $x < x_0$ and increasing. The function $S_2(y)$ has the same properties in the y-direction. The decaying solution (9) can be rewritten as

$$\widehat{E^{(z)}}(x, y, \omega) = e^{-i\omega\left(k_1\left(x+\frac{S_1(x)}{i\omega}\right)+k_2\left(y+\frac{S_2(y)}{i\omega}\right)\right)}. \tag{10}$$

Hence, this can formally be seen as a plane wave solution of the wave equation in the transformed variables $(\tilde{x}, \tilde{y})$, where

$$\tilde{x} = x + \frac{S_1(x)}{i\omega}, \qquad \tilde{y} = y + \frac{S_2(y)}{i\omega}.$$

Let $s_1(x, \omega) =: d\tilde{x}/dx = 1 + \frac{\sigma_1(x)}{i\omega}$ and $s_2(y, \omega) =: d\tilde{y}/dy = 1 + \frac{\sigma_2(y)}{i\omega}$, where $\sigma_1(x) = S_1'(x)$ and $\sigma_2(y) = S_2'(y)$. In terms of the original independent variables, the Fourier transformed wave equation in the $(\tilde{x}, \tilde{y})$ variables becomes

$$-\omega^2\widehat{E^{(z)}} = \frac{\partial^2 \widehat{E^{(z)}}}{\partial\tilde{x}^2} + \frac{\partial^2 \widehat{E^{(z)}}}{\partial\tilde{y}^2} =$$

$$\frac{1}{s_1(x, \omega)}\frac{\partial}{\partial x}\left(\frac{1}{s_1(x, \omega)}\frac{\partial\widehat{E^{(z)}}}{\partial x}\right) + \frac{1}{s_2(y, \omega)}\frac{\partial}{\partial y}\left(\frac{1}{s_2(y, \omega)}\frac{\partial\widehat{E^{(z)}}}{\partial y}\right). \tag{11}$$

Since s_1 does not depend on y and s_2 does not depend on x, we can rewrite (11) as

$$-s_1(x, \omega)s_2(y, \omega)\omega^2\widehat{E^{(z)}} = \frac{\partial}{\partial x}\left(\frac{s_2(y, \omega)}{s_1(x, \omega)}\frac{\partial\widehat{E^{(z)}}}{\partial x}\right) + \frac{\partial}{\partial y}\left(\frac{s_1(x, \omega)}{s_2(y, \omega)}\frac{\partial\widehat{E^{(z)}}}{\partial y}\right). \tag{12}$$

To transform back to the time domain, we introduce new dependent variables. There is some ambiguity in defining these variables but the important properties are that (12) is satisfied on the Fourier transformed side, and that the resulting PDE becomes well-posed. We start by noting that the left hand side of (12) can easily be transformed back to the time-domain, since

$$-s_1(x, \omega)s_2(y, \omega)\omega^2\widehat{E^{(z)}} = (i\omega + \sigma_1(x))(i\omega + \sigma_2(y))\widehat{E^{(z)}}.$$

To be able to transform back the last fractional expression in the right hand side of (12), we define $\widehat{H^{(x)}}$ according to

$$i\omega\widehat{H^{(x)}} = -\frac{s_1(x, \omega)}{s_2(y, \omega)}\frac{\partial\widehat{E^{(z)}}}{\partial y}.$$

Therefore,

$$(i\omega + \sigma_2(y))\widehat{H^{(x)}} = -\frac{\partial\widehat{E^{(z)}}}{\partial y} - \frac{\sigma_1(x)}{i\omega}\frac{\partial\widehat{E^{(z)}}}{\partial y}. \tag{13}$$

7

By also defining

$$i\omega\widehat{B^{(x)}} = -\frac{\partial \widehat{E^{(z)}}}{\partial y}, \tag{14}$$

we can transform back both (13) and (14) to the time-domain. We handle the other fractional expression in (12) in a corresponding way by introducing $H^{(y)}$ and $B^{(y)}$ according to

$$i\omega\widehat{H^{(y)}} = \frac{s_2(y,\omega)}{s_1(x,\omega)}\frac{\partial \widehat{E^{(z)}}}{\partial x}, \qquad i\omega\widehat{B^{(y)}} = \frac{\partial \widehat{E^{(z)}}}{\partial x}.$$

We apply the inverse Fourier transform and obtain the PML system

$$\begin{aligned}
\frac{\partial H^{(x)}}{\partial t} &= -\frac{\partial E^{(z)}}{\partial y} + \sigma_1(x)B^{(x)} - \sigma_2(y)H^{(x)}, \\
\frac{\partial B^{(x)}}{\partial t} &= -\frac{\partial E^{(z)}}{\partial y}, \\
\frac{\partial H^{(y)}}{\partial t} &= \frac{\partial E^{(z)}}{\partial x} + \sigma_2(y)B^{(y)} - \sigma_1(x)H^{(y)}, \\
\frac{\partial B^{(y)}}{\partial t} &= \frac{\partial E^{(z)}}{\partial x}, \\
\frac{\partial^2 E^{(z)}}{\partial t^2} &= \frac{\partial}{\partial x}\frac{\partial H^{(y)}}{\partial t} - \frac{\partial}{\partial y}\frac{\partial H^{(x)}}{\partial t} - (\sigma_1(x) + \sigma_2(y))\frac{\partial E^{(z)}}{\partial t} - \sigma_1(x)\sigma_2(y)E^{(z)}.
\end{aligned} \tag{15}$$

Substituting the time derivatives of $H^{(x)}$ and $H^{(y)}$ gives the modified wave equation

$$\begin{aligned}
\frac{\partial^2 E^{(z)}}{\partial t^2} = \Delta E^{(z)} &+ \frac{\partial}{\partial x}\left(\sigma_2(y)B^{(y)} - \sigma_1(x)H^{(y)}\right) - \frac{\partial}{\partial y}\left(\sigma_1(x)B^{(x)} - \sigma_2(y)H^{(x)}\right) \\
&- (\sigma_1(x) + \sigma_2(y))\frac{\partial E^{(z)}}{\partial t} - \sigma_1(x)\sigma_2(y)E^{(z)}.
\end{aligned}$$

We note in passing that the original un-damped wave equation is recovered outside the PML, where $\sigma_1 = 0$ and $\sigma_2 = 0$.

To investigate the well-posedness of (15) it is convenient to write it as a first order system, by introducing the variable D according to

$$\frac{\partial D}{\partial t} = \frac{\partial H^{(y)}}{\partial x} - \frac{\partial H^{(x)}}{\partial y} - \sigma_1(x)D. \tag{16}$$

Then,

$$\frac{\partial E^{(z)}}{\partial t} = \frac{\partial H^{(y)}}{\partial x} - \frac{\partial H^{(x)}}{\partial y} - \sigma_1(x)D - \sigma_2(y)E^{(z)}, \tag{17}$$

and the first four equations of (15) together with (16) and (17) can be written in the standard form

$$\frac{\partial \boldsymbol{w}}{\partial t} = A\boldsymbol{w}_x + B\boldsymbol{w}_y + C(x,y)\boldsymbol{w}. \tag{18}$$

8

One can show that the matrix

$$M = \kappa_1 A + \kappa_2 B, \quad \kappa_1 \text{ and } \kappa_2 \text{ real}, \ \kappa_1^2 + \kappa_2^2 = 1,$$

has real eigenvalues and a complete set of eigenvectors. The system (18) is therefore strongly hyperbolic, see [12]. However, because of the lower order term $C\boldsymbol{w}$, the system (18) can have solutions that grow in time.

In practical computations, the PML must be limited to a finite width $d > 0$, and boundary conditions must be applied at the outer boundary of the PML. Here we will simply set a homogeneous Dirichlet condition,

$$E^{(z)}(x, y, t) = 0, \quad (x, y) \in \Gamma_o, \ t \geq 0. \tag{19}$$

We also consider the wave equation in cylindrical coordinates (r, θ), where $x = r \cos \theta$, $y = r \sin \theta$. The derivation of the cylindrical PML equations can be done in exactly the same way as in the Cartesian case by the change of variables

$$\tilde{r} = r + \frac{S(r)}{i\omega},$$

see [16, 6] for details. In this case, the PML will have a circular interface to the interior domain. We define the interior as $\Omega_i = \{x^2 + y^2 < r_i^2\}$, for some fixed radius $r_i > 0$. Since we shall use a Cartesian grid, the computational domain is rectangular with $\Omega_c = [-r_i - d, r_i + d] \times [-r_i - d, r_i + d]$. In this case, the thickness of the PML varies between d and $\sqrt{2}d$. The resulting cylindrical PML equations, when transformed back to the time domain are

$$\frac{\partial B^{(x)}}{\partial t} = -\frac{\partial E^{(z)}}{\partial y} - \bar{\sigma}(r)B^{(x)} + s(r)(-\sin^2\theta B^{(x)} + \sin\theta\cos\theta B^{(y)}),$$

$$\frac{\partial H^{(x)}}{\partial t} = -\frac{\partial E^{(z)}}{\partial y} + s(r)((\cos^2\theta - \sin^2\theta)B^{(x)} + 2\sin\theta\cos\theta B^{(y)}),$$

$$\frac{\partial B^{(y)}}{\partial t} = \frac{\partial E^{(z)}}{\partial x} - \bar{\sigma}(r)B^{(y)} + s(r)(-\cos^2\theta B^{(y)} + \sin\theta\cos\theta B^{(x)}), \tag{20}$$

$$\frac{\partial H^{(y)}}{\partial t} = \frac{\partial E^{(z)}}{\partial x} + s(r)((\sin^2\theta - \cos^2\theta)B^{(y)} + 2\sin\theta\cos\theta B^{(x)}),$$

$$\frac{\partial^2 E^{(z)}}{\partial t^2} = \triangle E^{(z)} + \frac{\partial}{\partial x}(s(r)((\sin^2\theta - \cos^2\theta)B^{(y)} + 2\sin\theta\cos\theta B^{(x)}))$$

$$+ \frac{\partial}{\partial y}(s(r)((\sin^2\theta - \cos^2\theta)B^{(x)} - 2\sin\theta\cos\theta B^{(y)}))$$

$$- s(r)\frac{\partial}{\partial t}E^{(z)} - \sigma(r)\bar{\sigma}(r)E^{(z)}.$$

Here we have used the definitions

$$\bar{\sigma}(r) = \begin{cases} \frac{1}{r} \int_{r_i}^r \sigma(s)\,ds, & r > r_i, \\ 0, & r \leq r_i, \end{cases}$$

and

$$s(r) = \sigma(r) - \bar{\sigma}(r).$$

One advantage of the cylindrical PML is that $H^{(x)}$ and $H^{(y)}$ are not required in (20), whereas they must be computed in (15). However, if $H^{(x)}$ and $H^{(y)}$ are needed they can always be computed passively by integrating point-wise ODEs along with the other variables.

The PML/interior boundary is placed some distance outside of all perfectly conducting objects in the domain. The PML/interior boundary is determined by the location where σ changes from zero to a positive value, and is hence implicit in the method. For simplicity, the systems (15) and (20) are solved in the entire computational domain Ω_c with $\sigma = 0$ in Ω_i.

3   Numerical approximation

We use centered second order accurate differences in space to discretize the PML systems (15) and (20). Since the wave propagation speed is the same in all directions, we discretize the equations on a uniform grid $x_i = ih$, $y_j = jh$, where $h > 0$ is the constant grid size. Time is discretized on a uniform grid with $t_n = nk$, where $k > 0$ is the constant time-step. The approximation of a field $u(x_i, y_j, t_n)$ is denoted $u_{i,j}^n$. The usual finite difference operators are defined by

$$D_+^{(i)} u_{i,j} = \frac{u_{i+1,j} - u_{i,j}}{h}, \quad D_-^{(i)} u_{i,j} = D_+^{(i)} u_{i-1,j}, \quad D_0^{(i)} u_{i,j} = \frac{1}{2}\left(D_+^{(i)} + D_-^{(i)}\right) u_{i,j}.$$

The j-direction operators $D_0^{(j)}, D_+^{(j)}$, and $D_-^{(j)}$ are defined in a corresponding way. The time integration is based on the technique developed in [13, 14, 15]. The second order time derivative in the wave equation for $E^{(z)}$ is discretized using a time-centered second divided difference, and the first order equations for $H^{(x)}$, $B^{(x)}$, $H^{(y)}$ and $B^{(y)}$ are discretized with a second order accurate Adam-Bashforth method. For the Cartesian PML system (15),

this leads to

$$\frac{B_{i,j}^{(x)^{n+1}} - B_{i,j}^{(x)^n}}{k} = -\frac{3}{2}D_0^{(j)}E_{i,j}^{(z)^n} + \frac{1}{2}D_0^{(j)}E_{i,j}^{(z)^{n-1}},$$

$$\frac{H_{i,j}^{(x)^{n+1}} - H_{i,j}^{(x)^n}}{k} = -\frac{3}{2}\left(D_0^{(j)}E_{i,j}^{(z)^n} + \sigma_2(y_j)H_{i,j}^{(x)^n} - \sigma_1(x_i)B_{i,j}^{(x)^n}\right)$$
$$+\frac{1}{2}\left(D_0^{(j)}E_{i,j}^{(z)^{n-1}} + \sigma_2(y_j)H_{i,j}^{(x)^{n-1}} - \sigma_1(x_i)B_{i,j}^{(x)^{n-1}}\right),$$

$$\frac{B_{i,j}^{(y)^{n+1}} - B_{i,j}^{(y)^n}}{k} = \frac{3}{2}D_0^{(i)}E_{i,j}^{(z)^n} - \frac{1}{2}D_0^{(i)}E_{i,j}^{(z)^{n-1}},$$

$$\frac{H_{i,j}^{(y)^{n+1}} - H_{i,j}^{(y)^n}}{k} = \frac{3}{2}\left(D_0^{(i)}E_{i,j}^{(z)^n} - \sigma_1(x_i)H_{i,j}^{(y)^n} + \sigma_2(y_j)B_{i,j}^{(y)^n}\right)$$
$$-\frac{1}{2}\left(D_0^{(i)}E_{i,j}^{(z)^{n-1}} - \sigma_1(x_i)H_{i,j}^{(y)^{n-1}} + \sigma_2(y_j)B_{i,j}^{(y)^{n-1}}\right), \quad (21)$$

$$\frac{E_{i,j}^{(z)^{n+1}} - 2E_{i,j}^{(z)^n} + E_{i,j}^{(z)^{n-1}}}{k^2} = \left(D_+^{(i)}D_-^{(i)}E_{i,j}^{(z)^n} + D_+^{(j)}D_-^{(j)}E_{i,j}^{(z)^n}\right)$$
$$+ D_0^{(i)}\left(\sigma_2(y_j)B_{i,j}^{(y)^n} - \sigma_1(x_i)H_{i,j}^{(y)^n}\right)$$
$$- D_0^{(j)}\left(\sigma_1(x_i)B_{i,j}^{(x)^n} - \sigma_2(y_j)H_{i,j}^{(x)^n}\right)$$
$$- (\sigma_1(x_i) + \sigma_2(y_j))\frac{E_{i,j}^{(z)^{n+1}} - E_{i,j}^{(z)^{n-1}}}{2k}$$
$$- \sigma_1(x_i)\sigma_2(y_j)E_{i,j}^{(z)^n} + \alpha h^3 d_{i,j}^n.$$

Note that an explicit expression for $E_{i,j}^{(z)^{n+1}}$ can easily be found from the last equation. The last expression in the last equation is a stabilizing term developed in the aforementioned papers by Kreiss, Petersson and Yström. Away from all boundaries, it simplifies to

$$d_{i,j}^n = \Delta_h^2\left(\frac{E_{i,j}^{(z)^n} - E_{i,j}^{(z)^{n-1}}}{k}\right), \quad \Delta_h^2 E_{i,j}^{(z)^n} = \left(D_+^{(i)}D_-^{(i)} + D_+^{(j)}D_-^{(j)}\right)^2 E_{i,j}^{(z)^n}.$$

When $\sigma = 0$, the stability restriction for the time step is

$$k \le Ch, \quad C \approx \frac{1}{\sqrt{2}}.$$

Since $\sigma \ne 0$ only introduces lower order damping terms, it does not change the time step restriction as long as σ is independent of h and h is sufficiently small.

As initial conditions, we give $E^{(z)}$, $\partial E^{(z)}/\partial t$, $B^{(x)}$, and $B^{(y)}$. Furthermore, we initially set $H^{(x)} = B^{(x)}$ and $H^{(y)} = B^{(y)}$. To start the three level time integration, the solution at time $-k$ is computed using a truncated Taylor-series expansion in time.
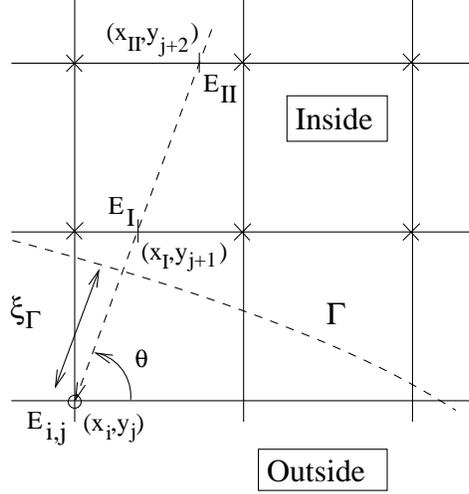
Figure 2: The points used for discretizing the Dirichlet boundary condition.

At the boundaries of the perfectly conducting objects, a Dirichlet boundary condition is imposed for $E^{(z)}$ using the method described in [13]. We only outline the technique here and refer to that paper for further details. We consider the inhomogeneous Dirichlet boundary condition

$$E^{(z)}(x, y, t) = f(x, y, t), \quad (x, y) \in \Gamma_i, \ t \geq 0.$$

The boundaries of the perfectly conducting objects are allowed to intersect the grid in an arbitrary manner. To be able to evaluate the right hand side of (21) at all grid points inside Ω_c, we use ghost points just outside the domain, see Figure 2. Let x_I, x_{II} be the intersections between the normal going through $\boldsymbol{x}_{i,j}$ and the grid lines $y = y_{j+1}$ and $y = y_{j+2}$, respectively. Denote by ξ_I, $\xi_{II} = 2\xi_I$ the distances between $\boldsymbol{x}_{i,j}$ and (x_I, y_{j+1}), (x_{II}, y_{j+2}), respectively. To aid in the approximation of the Dirichlet condition, we construct a Lagrange interpolant between three points along the normal: $(0, E^{(z)}_{i,j})$, $(\xi_I, E^{(z)}_I)$, $(\xi_{II}, E^{(z)}_{II})$,

$$Lv =: g_0(\xi_\Gamma)E^{(z)}_{i,j} + g_I(\xi_\Gamma)E^{(z)}_I + g_{II}(\xi_\Gamma)E^{(z)}_{II}, \tag{22}$$

where the coefficients are given by

$$g_0(\xi) = \frac{(\xi_I - \xi)(2\xi_I - \xi)}{2\xi_I^2}, \quad g_I(\xi) = \frac{\xi(2\xi_I - \xi)}{\xi_I^2}, \quad g_{II}(\xi) = \frac{\xi(\xi - \xi_I)}{2\xi_I^2}. \tag{23}$$

To approximate $E^{(z)}_I$ and $E^{(z)}_{II}$, we interpolate along the horizontal grid lines y_{j+1} and y_{j+2}:

$$E^{(z)}_I = c_1 E^{(z)}_{i,j+1} + c_2 E^{(z)}_{i+1,j+1} + c_3 E^{(z)}_{i+2,j+1}, \tag{24}$$

$$E^{(z)}_{II} = c_4 E^{(z)}_{i,j+2} + c_5 E^{(z)}_{i+1,j+2} + c_6 E^{(z)}_{i+2,j+2}. \tag{25}$$

12

where $c_k = \mathcal{O}(1)$ are the quadratic Lagrange interpolation coefficients. The interpolant is a third order approximation of the boundary value, i.e., $Lu(t) = u(\boldsymbol{x}_{i,j}^{\Gamma}, t) + \mathcal{O}(h^3)$, where $\boldsymbol{x}_{i,j}^{\Gamma}$ is the intersection point between the boundary and the normal going through the ghost point $\boldsymbol{x}_{i,j}$.

The interpolation formulas for $E_I^{(z)}$ and $E_{II}^{(z)}$, (24)-(25), hold when the angle θ between the normal and the x-axis satisfies $\pi/4 \leq \theta \leq \pi/2$. When $0 \leq \theta \leq \pi/4$, the horizontal interpolations are replaced by corresponding interpolations in the vertical direction. The expressions in the remaining three quadrants are simply obtained by reflections in index space, leading to a total of 8 different cases to treat all possible directions of the boundary.

When the normal is close to vertical (or horizontal), the boundary can intersect the grid such that ξ_{Γ} is arbitrarily close to ξ_I, i.e., $g_0(\xi_{\Gamma})$ can be arbitrarily close to zero. Hence, if (22) would be used to approximate the boundary condition, the time-stepping of (21) would become very stiff. To mitigate the stiffness, we add an artificial term to the interpolant (22) and consider instead

$$g_0(\xi_{\Gamma})E_{i,j}^{(z)} + g_I(\xi_{\Gamma})E_I^{(z)} + g_{II}(\xi_{\Gamma})E_{II}^{(z)} + \gamma(E_{i,j}^{(z)} - 2E_I^{(z)} + E_{II}^{(z)}) = f(\boldsymbol{x}_{i,j}^{\Gamma}, t), \qquad (26)$$

where the constant $\gamma > 0$. The artificial term is an undivided second difference in the normal direction so it inflicts an $\mathcal{O}(h^2)$ error in the boundary condition approximation. When the direction of the normal changes smoothly along the boundary, the error due to the artificial term also varies smoothly along the boundary. This situation is analyzed in [13] where it is shown that both the solution and its discrete gradient are second order accurate. That paper also shows that $\gamma = 0.25$ is an appropriate value for the coefficient of the artificial term.

Note that the extra variables $H^{(x)}$, $B^{(x)}$, $H^{(y)}$, and $B^{(y)}$ do not need boundary conditions on the perfectly conducting objects, since $\sigma_1 = \sigma_2 = 0$ in their vicinity.

4   Errors from the discretized PML equations

The error in the computed solution in the interior of the domain, e, comes from two sources,

$$e = e_1 + e_2.$$

The first component, e_1, denotes the difference between the solution of the continuous wave equation on the infinite domain and the solution of the continuous PML system on the truncated domain. The component e_2 is the error due to discretization of the continuous PML system on the truncated domain.

To estimate the error committed by truncating the PML, we first consider the Cartesian PML equations where the interior domain Ω_i is the half-plane $x < 0$, $\sigma_2(y) = 0$, and the PML is located in $0 \leq x \leq d$. After Fourier transforming in time and in the

y-direction,

$$\widehat{E^{(z)}}(x, y, \omega) = \frac{1}{\sqrt{2\pi}} \int_{-\infty}^{\infty} \widetilde{E^{(z)}}(x, \xi, \omega) e^{i\xi y} \, d\xi,$$

equations (12) and (19) become (note that $s_2 \equiv 1$ in this case)

$$-(\omega^2 - \xi^2)\widetilde{E^{(z)}} = \frac{1}{s_1(x,\omega)} \frac{\partial}{\partial x} \left(\frac{1}{s_1(x,\omega)} \frac{\partial \widetilde{E^{(z)}}}{\partial x} \right), \quad x \leq d, \tag{27}$$

$$\widetilde{E^{(z)}}(d, \xi, \omega) = 0. \tag{28}$$

We make the ansatz

$$\widetilde{E^{(z)}}(x) = A e^{ik\left(x + \frac{S_1}{i\omega}\right)} + B e^{-ik\left(x + \frac{S_1}{i\omega}\right)},$$

where $k = \sqrt{\omega^2 - \xi^2}$. Note that $B \neq 0$ corresponds to an incident wave traveling from the interior of the domain into the PML, while $A \neq 0$ is a spurious reflected wave traveling in the opposite direction. The boundary condition (28) gives

$$A = -B e^{-2ikd} e^{-2\frac{k}{\omega} S_1(d)}.$$

Hence, in the interior domain $(x < 0)$, the error from truncating the PML to a finite width $d > 0$ is given by

$$\widetilde{e}_1(x, \xi, \omega) = B e^{ik(x-2d)} e^{-2\frac{k}{\omega} \int_0^d \sigma_1(s) \, ds}, \quad x < 0. \tag{29}$$

When $\omega^2 \geq \xi^2$, k is real-valued and we set

$$\frac{k}{\omega} = \cos \theta,$$

where θ is the angle of the incident wave on the PML/interior interface. Hence, glancing waves, where $|\cos \theta| \sim 0$, get the smallest damping by the PML. Also note that the amplitude of the reflected wave only depends on the integral of $\sigma_1(x)$, but not on its specific shape.

For the cylindrical PML equations, we can calculate the errors due to truncating the PML for the case when a plane wave of frequency ω is scattered by a circular disc with radius a. We can write an outwardly propagating traveling wave solution of Maxwell's equations in terms of a series expansion,

$$\widehat{\mathcal{E}^{(z)}}(r, \theta, \omega) = \sum_{m=-\infty}^{\infty} A_m H_m^{(2)}(|\omega|r) e^{im\theta}. \tag{30}$$

Here $H_m^{(2)}$ are Hankel functions corresponding to outwardly propagating waves. In this expression, A_m are constants, determined from the boundary conditions. The coefficients in (30) representing the scattered field in an unbounded domain are (see [16])

$$A_m = -i^m \frac{J_m(|\omega|a)}{H_m^{(2)}(|\omega|a)}. \tag{31}$$

14

Here, J_m is the Bessel function of order m. The solution of the same scattering problem using the cylindrical PML equations (20) on a circular domain $\sqrt{x^2 + y^2} \leq r_o$, with the PML occupying the space $r_i < \sqrt{x^2 + y^2} < r_o$, can be represented as the following Bessel function expansion (see [16]),

$$\widehat{E^{(z)}}(r, \theta, \omega) = \sum_{m=-\infty}^{\infty} B_m(H_m^{(2)}(|\omega|\tilde{r}(r)) + R_m H_m^{(1)}(|\omega|\tilde{r}(r)))e^{im\theta}, \tag{32}$$

where the reflection coefficients are

$$R_m = -\frac{H_m^{(2)}(|\omega|\tilde{r}(r_o))}{H_m^{(1)}(|\omega|\tilde{r}(r_o))},$$

and the expansion coefficients are

$$B_m = -i^m \frac{J_m(|\omega|a)}{H_m^{(2)}(|\omega|a) + R_m H_m^{(1)}(|\omega|a)}.$$

Here $\tilde{r}$ is the transformed radial variable, definied by

$$\tilde{r}(r) = \begin{cases} r + \frac{1}{i\omega}\int_{r_i}^{r} \sigma(s)\, ds & r_i < r \leq r_o, \\ r & r \leq r_i. \end{cases}$$

In this case, the error due to truncating the PML to a finite width is obtained as the difference between the solutions (30) and (32). Again we see that the error is determined by the integral of $\sigma(r)$, even though the relation is more complicated than in the Cartesian case.

If the numerical approximation is stable, e_2 goes to zero as $h \to 0$, while e_1 goes to zero as the integral over σ gets larger, independently of the discretization. For given mesh sizes h and k, we must therefore design the PML so that e_1 does not dominate e_2. If we know the smallest value of h and the largest incident wave angle (that minimizes $\cos\theta$), we can select the width of the layer, d, or scale σ to make the integral of σ big enough. However, it is not possible to use the same σ and d independently of the grid size if we want a method where the error decreases as $\mathcal{O}(h^p)$ when $h \to 0$. In particular, we are interested in adjusting the properties of the PML so that e_1 goes to zero at the same rate as e_2 when $h \to 0$.

If we are using a p'th order accurate discretization scheme, e_2 is of the order $\mathcal{O}(h^p)$, and we also want $e_1 = \mathcal{O}(h^p)$. Hence, in order for e_1 to stay of the same order as e_2, we must have

$$\int_0^d \sigma_1(x_0 + s)\, ds \geq \frac{p}{2\cos\theta}|\log h|, \tag{33}$$

where we assumed that the PML layer is located at $x_0 \leq x \leq x_0 + d$. To satisfy (33), the PML thickness d and/or σ must change with h. That means that there is no fixed

PDE with which the PML system is consistent, and we can not rely on standard results for approximation of PDEs to understand the convergence properties of the numerical approximation. One possibility, which we will explore below, is to make σ proportional to $|\log h|$ and let the layer thickness be fixed. Note that the largest possible σ under the explicit time-stepping constraint $k/h < \text{const.}$ is $\sigma = \mathcal{O}(1/h)$. By using such a large σ, one could even allow the thickness of the PML to decrease as $h \to 0$ and still satisfy (33). However, scaling σ in this way means that σ becomes poorly resolved on the grid as $h \to 0$, which in turn increases the discretization error e_2. Our numerical experiments will confirm this hypothesis and show that a $\sigma = \mathcal{O}(1/h)$ results in numerical inaccuracies, which reduce the convergence rate.

4.1 Discretization error for large σ

We here investigate the convergence rate of the discretization error e_2, when σ is allowed to grow with h. For simplicity, we limit our investigation to the one-dimensional case and study the system (3). The exact plane wave solution is

$$E^{(z)}(x,t) = A\left(-e^{i\omega(t+x-2d)+\int_0^x \sigma(s)\,ds - 2\int_0^d \sigma(s)\,ds} + e^{i\omega(t-x)-\int_0^x \sigma(s)\,ds}\right) \tag{34}$$

$$H^{(y)}(x,t) = A\left(-e^{i\omega(t+x-2d)+\int_0^x \sigma(s)\,ds - 2\int_0^d \sigma(s)\,ds} - e^{i\omega(t-x)-\int_0^x \sigma(s)\,ds}\right). \tag{35}$$

Here A is an arbitrary amplitude of the wave. Note that $E^{(z)}$ is bounded independently of σ. In our computations below, we have used an approximation which before time discretization corresponds to

$$\frac{dH_j^{(y)}(t)}{dt} = D_0 E_j^{(z)} - \sigma_j H_j^{(y)}, \qquad\qquad j = \ldots, -2, -1, \tag{36}$$

$$\frac{d^2 E_j^{(z)}(t)}{dt^2} = D_+ D_- E_j^{(z)} - \sigma_j \frac{dE_j^{(z)}}{dt} - D_0(\sigma_j H_j^{(y)}), \quad j = \ldots, -2, -1. \tag{37}$$

We have been unable to find an energy estimate for the above node-centered discretization and will here instead analyze the staggered approximation

$$\frac{dH_{j-1/2}^{(y)}(t)}{dt} = D_- E_j^{(z)} - \sigma_{j-1/2} H_{j-1/2}^{(y)}, \qquad j = \ldots, -1, 0,$$

$$\frac{dE_j^{(z)}(t)}{dt} = D_+ H_{j-1/2}^{(y)} - \sigma_j E_j^{(z)}, \qquad j = \ldots, -2, -1. \tag{38}$$

$$E_0^{(z)}(t) = 0.$$

The corresponding second order equation for $E_j^{(z)}$ is

$$\frac{d^2 E_j^{(z)}(t)}{dt^2} = D_+ D_- E_j^{(z)} - \sigma_j \frac{dE_j^{(z)}}{dt} - D_+(\sigma_{j-1/2} H_{j-1/2}^{(y)}),$$

16

which shows that the node-centered and staggered schemes only differ in how $\partial(\sigma H^{(y)})/\partial x$ is discretized. The grid points are located at $x_j = d + jh$, with $j = \dots, -3, -2, -1, 0$. The differences between the solution of the continuous problem (3) and the discrete approximation (38) are denoted $e_j(t) = E^{(z)}(x_j, t) - E_j^{(z)}(t)$ and $f_{j-1/2}(t) = H^{(y)}(x_{j-1/2}, t) - H_{j-1/2}^{(y)}(t)$. Inserting these into (38) gives the error equation

$$
\begin{aligned}
\frac{df_{j-1/2}(t)}{dt} &= D_- e_j - \sigma_{j-1/2} f_{j-1/2} + \tau_{j-1/2}^H, \quad & j &= \dots, -1, 0, \\
\frac{de_j(t)}{dt} &= D_+ f_{j-1/2} - \sigma_j e_j + \tau_j^E, \quad & j &= \dots, -2, -1, \\
e_0(t) &= 0,
\end{aligned}
\tag{39}
$$

where the local truncation errors are

$$
\begin{aligned}
\tau_{j-1/2}^H &=: -\frac{\partial H^{(y)}(x_{j-1/2}, t)}{\partial t} + D_- E^{(z)}(x_j, t) - \sigma_{j-1/2} H^{(y)}(x_{j-1/2}, t) \\
&= \frac{h^2}{24} E_{xxx}^{(z)}(x_{j-1/2} + \phi_1 h, t),
\end{aligned}
\tag{40}
$$

$$
\begin{aligned}
\tau_j^E &=: -\frac{\partial E^{(z)}(x_j, t)}{\partial t} + D_+ H^{(y)}(x_{j-1/2}, t) - \sigma_j E^{(z)}(x_j, t) \\
&= \frac{h^2}{24} H_{xxx}^{(y)}(x_j + \phi_2 h, t).
\end{aligned}
\tag{41}
$$

Taylor expansion of the divided differences were used to arrive at the final expressions. The third derivatives in the right hand side are evaluated at some intermediate points with $0 < \phi_1, \phi_2 < 1$.

We consider the case when the exact solution is the plane wave given by (34), (35). and insert that solution into the truncation error. After a lengthy but straightforward calculation we obtain

$$
E_{xxx}^{(z)}(x, t) = ((\sigma'' + (i\omega + \sigma)^3) H^{(y)}(x, t) + 3(i\omega + \sigma)\sigma' E^{(z)}(x, t))
\tag{42}
$$

$$
H_{xxx}^{(y)}(x, t) = ((\sigma'' + (i\omega + \sigma)^3) E^{(z)}(x, t) + 3(i\omega + \sigma)\sigma' H^{(y)}(x, t))
\tag{43}
$$

If the method is stable, the local truncation errors determine the convergence rate. One subtle point is that stability must hold also when σ depends on h. We will estimate the error of the staggered scheme (38) using a weighted 2-norm, which allows us to take the norm of functions which are bounded but do not go to zero at $-\infty$. Let $\alpha(x) > 0$ and define

$$
||u||_\alpha^2 = h \sum_{j=-\infty}^{0} \alpha(x_j) u_j \bar{u}_j
$$

satisfying

$$
\sum_{j=-\infty}^{0} \alpha(x_j) < \infty
$$

17

and $\alpha'(x)/\alpha(x)$ bounded. We also require that $\alpha(x) = 1$ for $x > -L$, where $L \gg 1$ is a constant. The scalar product corresponding to the norm is

$$(u, v)_\alpha = \sum_{j=-\infty}^{0} \alpha(x_j) u_j \bar{v}_j h,$$

For staggered grid functions, we use the convention that $u_{j-1/2}$ is used instead of u_j. An example of a weight function satisfying these criteria is

$$\alpha(x) = \begin{cases} 1, & x \geq -L, \\ e^{x+L}, & x < -L. \end{cases}$$

Lemma 1 *Let $e_0 = 0$, assume that $\alpha'(x) > 0$, $\alpha''(x) > 0$, and that*

$$\alpha'(x)/\alpha(x) < c_1$$

for some constant c_1. Furthermore, let the grid size satisfy $h < 1/(2c_1)$. Then,

$$(f, D_- e)_\alpha + (D_+ f, e)_\alpha \leq \frac{3c_1}{2}(||e||_\alpha^2 + ||f||_\alpha^2).$$

Proof: The following calculations are straightforward:

$$(f, D_- e)_\alpha + (D_+ f, e)_\alpha = \sum_{j=-\infty}^{0} \alpha_j f_{j-1/2}(e_j - e_{j-1}) + \sum_{j=-\infty}^{0} \alpha_j e_j (f_{j+1/2} - f_{j-1/2})$$

$$= -\sum_{j=-\infty}^{0} (\alpha_j - \alpha_{j-1}) e_{j-1} f_{j-1/2} = -\sum_{j=-\infty}^{0} \frac{(\alpha_j - \alpha_{j-1})}{h\sqrt{\alpha_j \alpha_{j-1}}} h \sqrt{\alpha_{j-1}} e_{j-1} \sqrt{\alpha_j} f_{j-1/2}$$

$$\leq \max_j \frac{(\alpha_j - \alpha_{j-1})}{h\sqrt{\alpha_j \alpha_{j-1}}} ||e||_\alpha ||f||_\alpha \leq \max_j \frac{(\alpha_j - \alpha_{j-1})}{h\sqrt{\alpha_j \alpha_{j-1}}} \frac{1}{2}(||e||_\alpha^2 + ||f||_\alpha^2) \qquad (44)$$

It remains to estimate

$$\frac{(\alpha_j - \alpha_{j-1})}{\sqrt{\alpha_j \alpha_{j-1}}} = \sqrt{\frac{\alpha(x)}{\alpha(x-h)}} - \sqrt{\frac{\alpha(x-h)}{\alpha(x)}}.$$

We first prove

$$1 - hc_1 \leq \frac{\alpha(x-h)}{\alpha(x)} \leq 1.$$

The upper limit is obvious, since the function is increasing. The lower limit follows from

$$\alpha(x) - \alpha(x-h) = \int_{x-h}^{x} \alpha'(s)\, ds \leq h\alpha'(x) \leq h\frac{\alpha'(x)}{\alpha(x)}\alpha(x) \leq hc_1\alpha(x)$$

18

where $\alpha''(x) > 0$ is needed to estimate the integral. Dividing by $\alpha(x)$ (which is positive) gives

$$1 - hc_1 \leq \frac{\alpha(x - h)}{\alpha(x)}$$

and since $1 - hc_1 \leq \sqrt{1 - hc_1}$, the same lower bound can be used for the square root of $\alpha(x - h)/\alpha(x)$. We obtain the estimate

$$\sqrt{\frac{\alpha(x)}{\alpha(x - h)}} - \sqrt{\frac{\alpha(x - h)}{\alpha(x)}} \leq \frac{1}{1 - hc_1} - 1 + hc_1 \leq 1 + 2hc_1 - 1 + hc_1 = 3hc_1 \qquad (45)$$

where we used that $1/(1 - x) < 1 + 2x$ for $x < 1/2$. Using (45) in (44) gives the desired result and concludes the proof of the lemma.

We can now prove

Theorem 1 *Assume that $\sigma(x) = P(x)\sigma_{max} \geq 0$, where $P(x)$ and its first two derivatives are bounded independently of h, but σ_{max} is allowed to grow as $h \to 0$. Then,*

$$||e(t)||_\alpha + ||f(t)||_\alpha \leq Ch^2(1 + \sigma_{max}^3)e^{c_2 t}.$$

Here C and c_2 are constants independent of h and σ_{max}.

Proof: Lemma 1 is used to obtain the following norm estimate for (39)

$$\frac{1}{2}\frac{d}{dt}(||e(t)||_\alpha^2 + ||f(t)||_\alpha^2) =$$

$$(f, D_- e)_\alpha + (D_+ f, e)_\alpha - (f, \sigma f)_\alpha - (e, \sigma e)_\alpha + (f, \tau^H)_\alpha + (e, \tau^E)_\alpha$$

$$\leq \frac{3c_1}{2}\left(||e||_\alpha^2 + ||f||_\alpha^2\right) + (f, \tau^H)_\alpha + (e, \tau^E)_\alpha$$

$$\leq \frac{3c_1 + 1}{2}\left(||f||_\alpha^2 + ||e||_\alpha^2\right) + \frac{1}{2}\left(||\tau^H||_\alpha^2 + ||\tau^E||_\alpha^2\right)$$

The assumption $\sigma(x) \geq 0$ was used to remove the terms $(f, \sigma f)_\alpha$ and $(e, \sigma e)_\alpha$ from the estimate. Gronwall's Lemma gives (after taking the square root)

$$||e(t)||_\alpha + ||f(t)||_\alpha \leq Ce^{c_2 t} \max_{0 < s < t}(||\tau^H(s)||_\alpha + ||\tau^E(s)||_\alpha),$$

where we have assumed that the errors are initially zero. Here C and c_2 are constants independent of h and t. The error in the solution is thus bounded by the size of the truncation error. Assuming that all derivatives of $P(x)$ up to second order are bounded in (43), we obtain

$$||\tau^H||_\alpha + ||\tau^E||_\alpha \leq Ch^2(1 + \sigma_{max}^3)$$

with C independent of h. C depends on $P(x)$ and its first two derivatives, C also depends on ω and the wave amplitude. We used that $H^{(y)}$ and $E^{(z)}$ given by (34), (35) are bounded. This concludes the proof of the theorem.

19

The theorem tells us that we can let σ_{max} increase as $|\log h|$, and still maintain almost second order accurate convergence. A faster increase of σ_{max} could lead to slower convergence or divergence.

As was mentioned above, we have not been successful in finding a similar norm estimate for the node-centered scheme (36), (37). However, the truncation error for that approximation is

$$\tau_j^E = \frac{h^2}{12}((\sigma''' + 6(i\omega + \sigma)^2\sigma')H^{(y)} + (3(\sigma')^2 + 4(i\omega + \sigma)\sigma'' + (i\omega + \sigma)^4)E^{(z)}),$$

and a corresponding expression for τ^H. Hence, if the method is stable, the corresponding requirement for $P(x)$ is that it must have three continuous derivatives, bounded independently of h. The convergence rate is in that case determined by $h^2\sigma_{max}^4$. For this reason, we use a σ with three continuous derivatives in the numerical examples below. In Section 5, we shall demonstrate the close to second order convergence rate obtained when σ_{max} increases as $|\log h|$.

5   Numerical examples

The discussion in the previous sections will here be illustrated by numerical experiments. In the first example, we study the effect from a single PML. The domain is of size $-2 < x < d$, $-2 < y < 2$. Periodic boundary conditions are used in the y-direction. The PML is only acting in the x-direction, and is located at $0 < x < d$, where d is the layer width. The problem setup is depicted in Figure 3. The incident plane wave $E^{(z)} = \sin(\pi(t - x - y))$ is imposed as a Dirichlet boundary condition on the left boundary. This wave travels into the PML interface at an angle $\theta = \pi/4$. As absorbing function, we use

$$\sigma_1(x) = P_7(x/d_w)\sigma_{max},$$

where $P_7(s)$ is the piecewise polynomial

$$P_7(s) = \begin{cases} 0, & s \leq 0, \\ c_7 \int_0^s q^3(1-q)^3 \, dq, & 0 < s < 1, \\ 1, & s \geq 1. \end{cases}$$

The constant c_7 normalizes the integral so that $P_7(s)$ becomes continuous at $s = 1$. The transition width is in this example $d_w = 1/2$. This σ is a function that increases from 0 to σ_{max} over a transition zone of length $1/2$, and then stays at the constant value σ_{max}. There are three continuous derivatives at the break points $x = 0$ and $x = 1/2$. Here σ_{max} is a constant which represents the strength of the PML. A grid convergence study for the case $d = 2$ is shown in Figure 4. We show the time evolution of the error, i.e., the difference in maximum norm between the computed solution and the exact solution on an
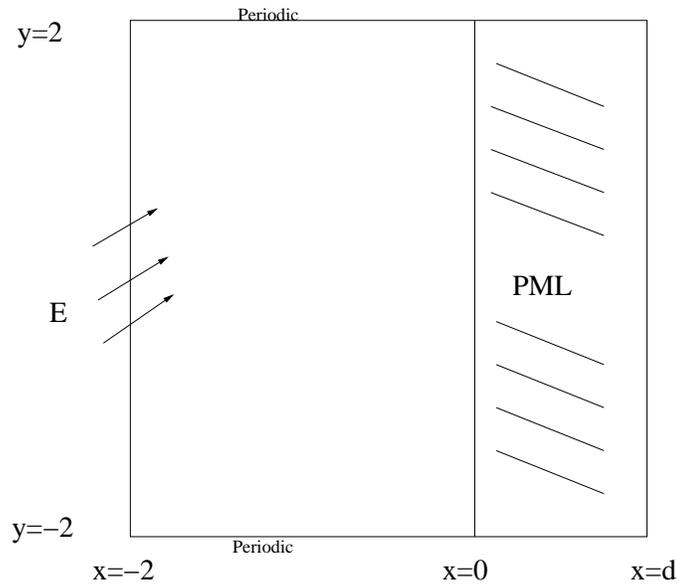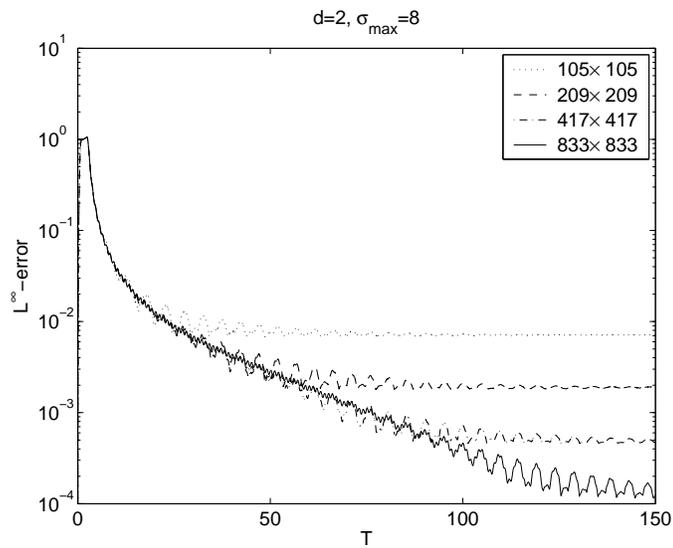
Figure 3: The first test problem.

Figure 4: Error vs. time for PML thickness $d = 2$ and constant $\sigma_{max} = 8.0$ on a sequence of refined grids.
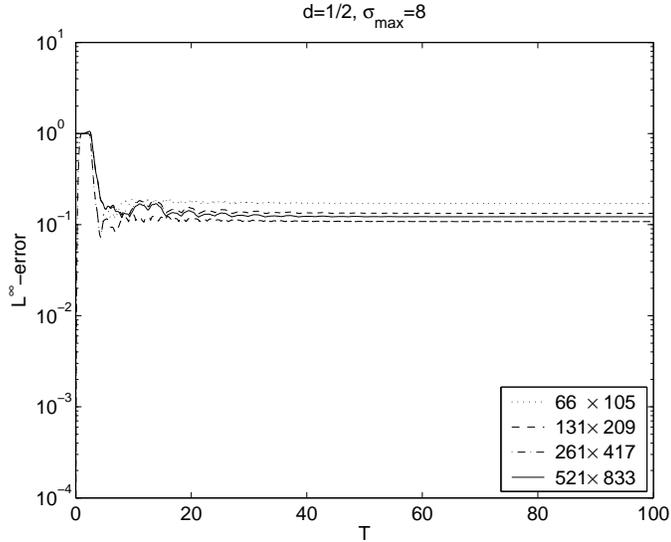
Figure 5: Error vs. time with PML thickness $d = 1/2$ and constant $\sigma_{max} = 8.0$ for a sequence of refined grids.

infinite domain, evaluated on $[-2, 0] \times [-2, 2]$. The initial data is zero everywhere, which explains why the error initially is of the order $\mathcal{O}(1)$. To avoid unnecessary transients, the Dirichlet forcing is smoothly turned on at the left boundary, and at time $t = 2$ it is fully developed. Since the frequency and wave number of the exact solution are known, formula (29) can be used to estimate the PML modelling error to be $e_1 \approx 2 \times 10^{-9}$. In Figure 4 we see that the total error is dominated by the numerical discretization error, e_2, and we observe a second order accurate behavior using the present range of grid sizes. The coarsest grid has 105×105 points, which corresponds to $h = 0.0385$. All computations in this section have the same coarsest h. The refinements are obtained by successive factor of 2 reductions of h.

Results from the same computation, but with $d = 1/2$, are shown in Figure 5. Here the estimated e_1 error level is 6×10^{-2}, which explains why the total error stays constant when the grid is refined. The coarsest grid has 66×105 grid points, which corresponds to the same grid size as in the previous example. The number of points is smaller in the x-direction, because the smaller d makes the computational domain shorter.

The results in Figure 4 and Figure 5 are not surprising. The difference scheme converges and reproduces the properties of the the PML system of PDEs. Next we will let σ_{max} and/or the width of the layer vary with h. In Figure 6 we show the behavior of the total error in the computed solution when

$$\sigma_{max} = 5.6569|\log h| - 2.1357$$

and the layer width $d = 1/2$. The expression for σ_{max} is selected so that $\sigma_{max} = 8$ on the coarsest grid, and so that (29) gives second order accurate convergence of e_1 for the angle
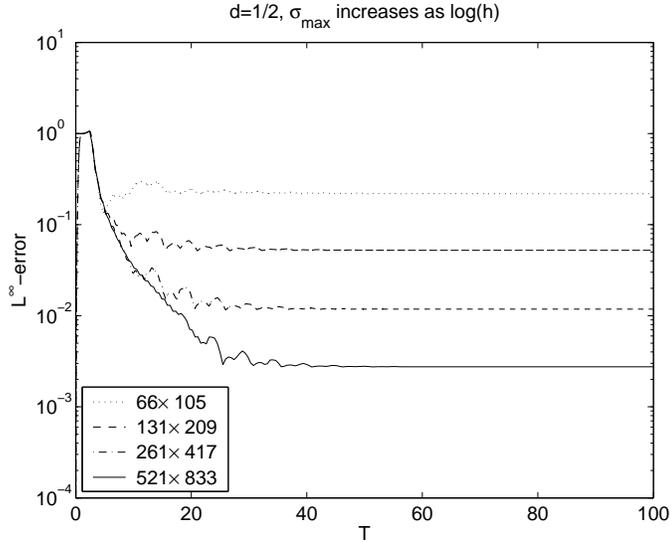
22

Figure 6: Error vs. time with PML thickness $d = 1/2$ for a sequence of refined grids with logarithmically increasing σ_{max}.

of incidence $\pi/4$. The grids in Figure 6 are the same as in Figure 5, and σ_{max} are equal on the coarsest grid in both figures. Note that the error decreases as $\mathcal{O}(h^2)$ in Figure 6.

According to the heuristic discussion above, second order error convergence could be obtained by fixing σ_{max}, and instead use an expanding layer. In Figure 7, we show a numerical experiment with a logarithmically expanding PML. The above computation is repeated, but now with $\sigma_{max} = 8$, and the layer width $d = d_0|\log h| + d_1$. The constants d_0 and d_1 are chosen so that $d = 1/2$ on the coarsest grid and so that e_1 according to formula (29) decreases as $\mathcal{O}(h^2)$. Conclusion: this also works, but is more expensive since the computational domain gets larger as $h \to 0$.

Finally, we make a numerical experiment to show what happens if σ is chosen too large. We solve the same problem as above, but with a fixed number of grid points in the PML. Having a fixed number of grid points means that d decreases as $\mathcal{O}(h)$ when the grid is refined. It is therefore necessary to increase σ_{max} as $|\log h|/h$ in order to make the modeling error e_1 go to zero. The results in Figure 8 were obtained using 10 grid points in the PML, the transition width $d_w = d$, and setting $\sigma_{max} = 0.2316|\log h|/h$. As before, the total error was evaluated in $-2 \le x \le 0$, $-2 \le y \le 2$. This corresponds to $\sigma_{max} = 20$ on the coarsest grid (105×63 grid points). The value $\sigma_{max} = 20$ was chosen because it gave the smallest error when several different σ_{max} values were tried on the coarse grid. Note that the smallest error in Figure 8 is obtained on the coarsest grid and the error increases as the grid is refined. Also note that this $\sigma(x)$ corresponds to a $P(x)$ where $P'(x) = \mathcal{O}(1/h)$ and $P''(x) = \mathcal{O}(1/h^2)$, which violates the assumptions of Theorem 1. However, the error increases slower than the rate given by the bound in
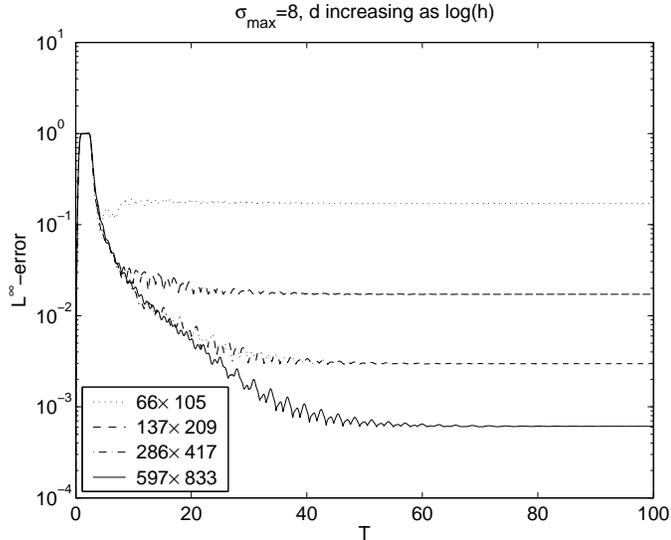
23

Figure 7: Error vs. time for a sequence of refined grids with logarithmically increasing PML thickness and constant $\sigma_{max} = 8.0$.

Theorem 1. Of course, the theorem only provides an upper bound on the growth and there is no guarantee that the bound is sharp. Furthermore, the norm in Theorem 1 is taken over the entire computational domain, but the total error is only evaluated in the interior of the domain (not including the PML).

5.1 Scattering

We here consider a standard test problem: scattering from a disk due to an incident plane wave. We solve the equations for the scattered field by subtracting out the incident plane wave from the equations. The incident wave only affects the computation through the boundary forcing on the disk. We will consider both the PML in Cartesian coordinates (15) as well as the cylindrical PML (20).

In our example, the incident wave is $\mathcal{E}^{(z)}{}_{inc} = \cos(\omega(t-x))$, where $\omega = 5$. The scatterer is a disk of radius 0.5 (i.e., $a = 0.5$ in (31)) represented as an embedded boundary in a uniform Cartesian grid. The problem setup is outlined in Figure 9. For the Cartesian PML, the interior domain is $-3 < x < 3$, $-3 < y < 3$, and a PML of thickness d is added, making the total domain $-3 - d < x < 3 + d$, $-3 - d < y < 3 + d$. For the cylindrical PML, we use a circular PML/interior interface with radius 3, but the total computational domain is rectangular. Therefore, the solution formula (32) is not directly applicable, but since the circular domain with $r_o = 3 + d$ is included in our computational domain, applying (32) with $r_o = 3 + d$ and $r_i = 3$ should overestimate the error e_1.

A computed solution is displayed in Figure 10. Initially all fields are zero, and the
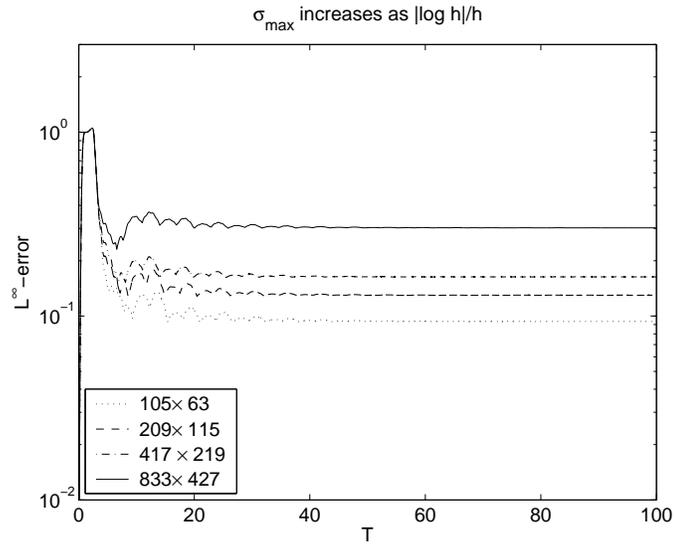
24

Figure 8: Error vs. time for a sequence of refined grids with fixed number of points in the PML and σ_{max} increasing as $\log h/h$. Note that the error increases as the grid is refined.
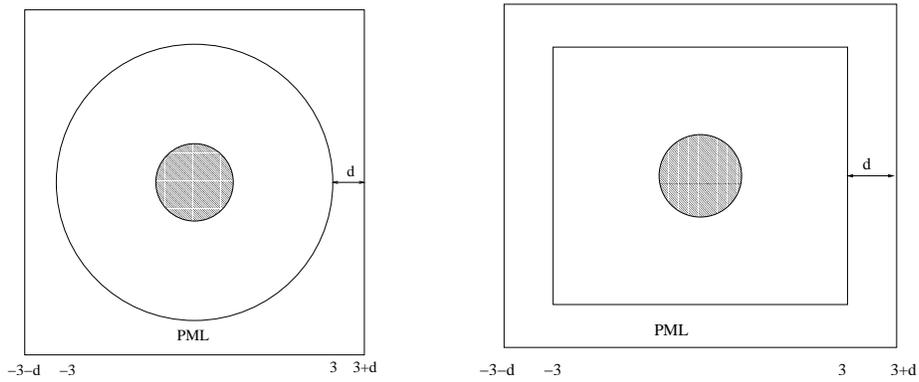

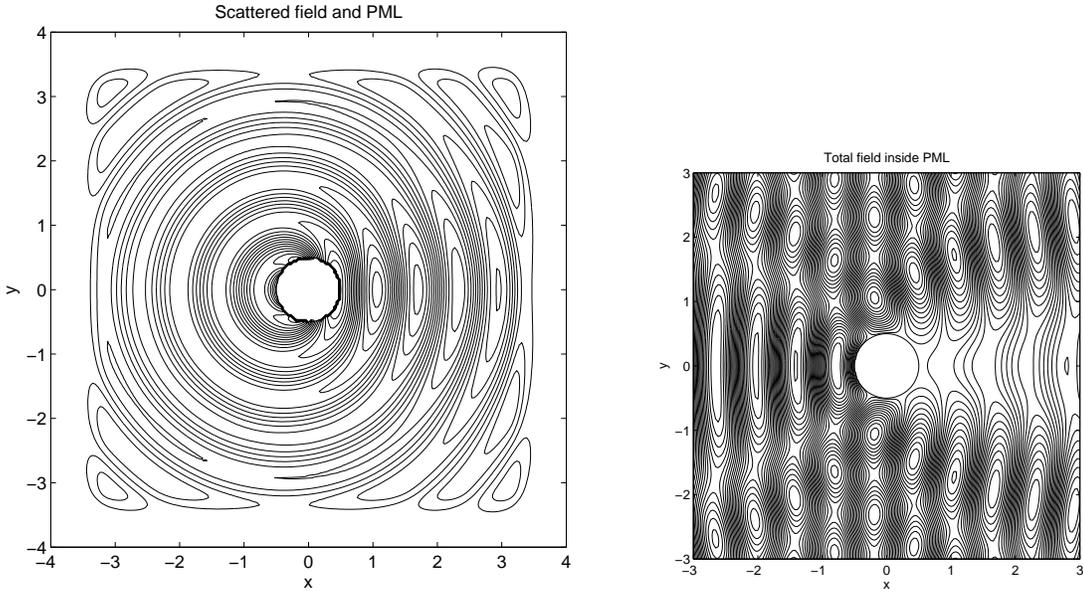Figure 9: Second test problem. Cylindrical PML (left) and Cartesian PML (right).

Figure 10: Computed scattered field including PML (left), corresponding total field excluding PML (right).

scatter field is smoothly turned on by giving the boundary data

$$E^{(z)} = -(1 - e^{-5t^3})\mathcal{E}^{(z)}{}_{inc}, \quad \text{on } \Gamma_i,$$

on the disk boundary. The scattering object is perfectly conducting, so the total field on the physical boundary is zero. Since we solve for the scattered field, the boundary condition on the perfectly conducting cylinder is $E^{(z)} = -\mathcal{E}^{(z)}{}_{inc}$, which is satisfied to machine precision for $t \geq 2$. A time periodic solution is obtained after a transient phase.

In Figure 11, we display the norm of the error as a function of time for the cylindrical PML system (20), for grids of increasing refinement. Here we use $\sigma(r) = P_7((r - 3)/d_w)\sigma_{max}$, with $d_w = 1/2$, $\sigma_{max} = 10$, and $d = 1$. An expression for the function $\bar{\sigma}(r)$ was found by integrating P_7 analytically. The error is calculated as the difference between the computed solution, and the exact solution of the problem on the infinite domain, evaluated through the Bessel function expansion (30) with the coefficients (31). The error is measured in maximum norm over the interior domain, $0.5 < \sqrt{x^2 + y^2} < r_i = 3$. According to the solution formulae (30) and (32), the maximum norm of the e_1 component of the error is less than 10^{-6}. Figure 12 shows the same computation as Figure 11, but using the Cartesian PML equations. At the right boundary, the PML has $\sigma_1(x) = \sigma_{max}P_7((x - 3)/d_w)$, with $d_w = 1/2$ and $\sigma_{max} = 10$. The left, lower and upper boundaries are treated in a corresponding way. The convergences shown in Figure 11 (cylindrical PML) and in Figure 12 (Cartesian PML) are both second order accurate, since on all grids the total error
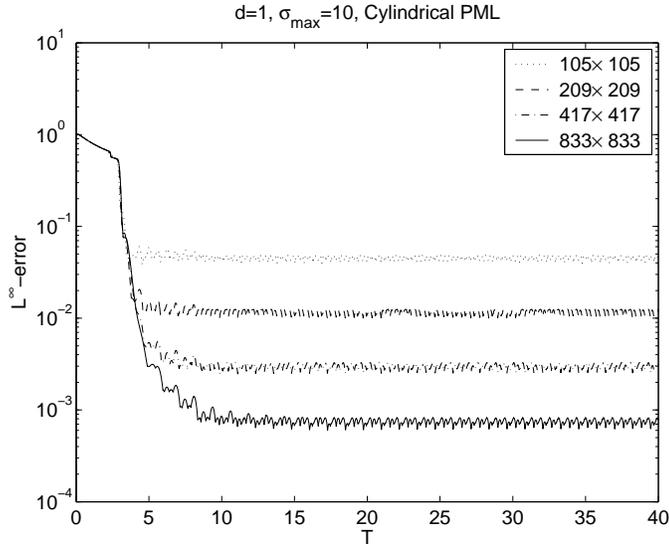
26

Figure 11: Error norm vs. time, cylindrical scatter. Cylindrical PML, $\sigma_{max} = 10$, $d = 1$.

is larger than the estimated e_1 level. Thus the discretization error dominates.

In contrast, the convergences shown in Figure 13 (cylindrical PML) and Figure 14 (Cartesian PML) were obtained using $\sigma_{max} = 3$, thus increasing the error due to truncating the PML to $e_1 \approx 3.48 \times 10^{-2}$. This change is large enough to let e_1 dominate the discretization error e_2 on the finer grids and the effect is clearly seen.

We next study grid convergence when $\sigma_{max} = c_1 |\log h| + c_2$. In this example, c_1 and c_2 are chosen such that σ_{max} is 3 on the coarsest grid and that (33) is satisfied for angles up to $\pi/4$. A careful measurement of the results in Figures 15 and 16 verify that second order convergence is obtained for both the cylindrical and the Cartesian PML equations.

5.2 Capabilities of the embedded boundary method

In this section we show a few examples of scattering from various objects. The purpose of these computations is to demonstrate the capabilities of the embedded boundary method.

The method was implemented for parallel computing using the MPI library. Operations related to boundary conditions on the embedded boundary are local, so that parallelization is just as straightforward as for an explicit finite difference algorithm. The arrays are distributed uniformly with an equal number of grid points in each processor. The grid points inside the objects are not used, and therefore the load balance is not perfect. Nevertheless, the method works well and considerable speed-up can be achieved. An example of speed-up is shown in Figure 17, where the cylinder scatter problem was solved with 833×833 grid points on a cluster of Itanium 2 nodes connected by a Myrinet-2000
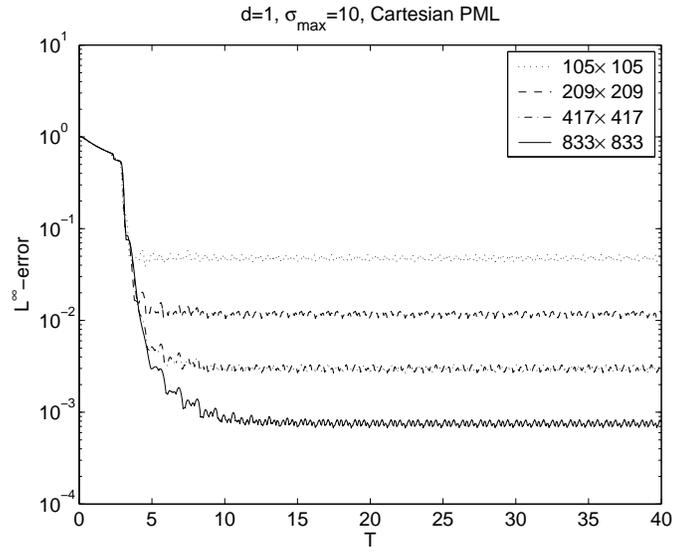
27

Figure 12: Error norm vs. time, cylindrical scatter. Cartesian PML, $\sigma_{max} = 10$, $d = 1$.
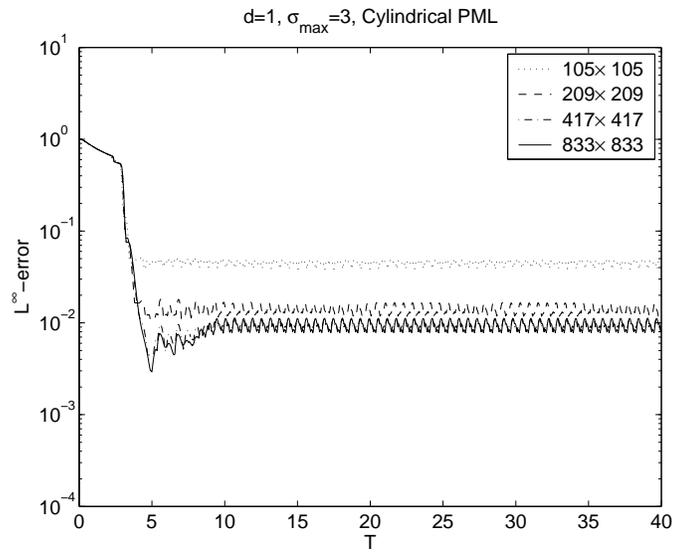

Figure 13: Error norm vs. time, cylindrical scatter. Cylindrical PML, $\sigma_{max} = 3$, $d = 1$.
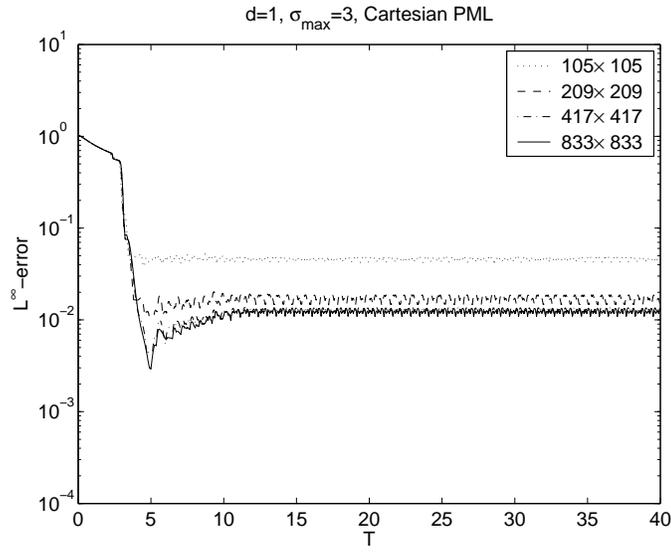
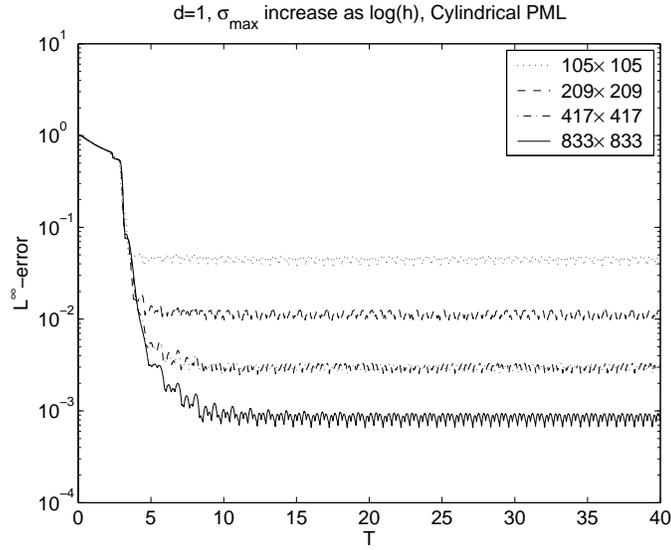Figure 14: Error norm vs. time, cylindrical scatter. Cartesian PML, $\sigma_{max} = 3$, $d = 1$.

Figure 15: Error norm vs. time, cylindrical scatter. Cylindrical PML, σ_{max} increases logarithmically with h, $d = 1$.
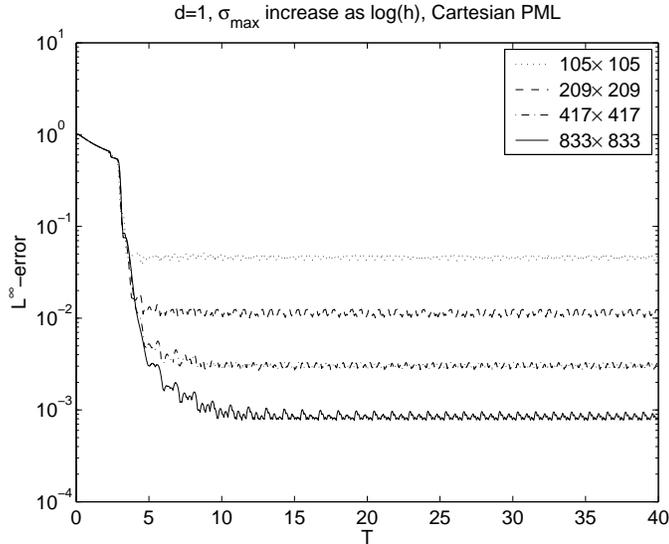
29

Figure 16: Error norm vs. time, cylindrical scatter. Cartesian PML, σ_{max} increases logarithmically with h, $d = 1$.

switch. The solid line shows the speed up actually measured using up to 20 processors. Perfect speed up is represented by the dashed line.

In Figure 18 we show scattering from a horseshoe shaped object. Contour lines of the total $E^{(z)}$ field is plotted on $[-3, 3] \times [-3, 3]$. The total computational domain was $[-4, 4] \times [-4, 4]$ with the PML occupying $-4 < x < -3$, $3 < x < 4$, $-4 < y < -3$, and $3 < y < 4$. The incoming plane wave had $\omega = 15$ and 209×209 grid points were used. The solution was computed to time 25. The boundary of the object is a periodic cubic spline curve, which was obtained by interpolation through a few specified boundary points.

With the embedded grid technique, it is straightforward to place more than one object in the computational domain. An example of this is the scattering from three cylinders, shown in Figure 19. Contour lines of the total $E^{(z)}$ field are shown. Except for the geometry, all computational parameters were the same as for the computation in Figure 18.

Finally, Figure 20 shows scattering from an unidentified object. Contour lines of the $E^{(z)}$ field are shown. The incident plane wave is tilted an angle 25.8 degrees and has $\omega = 15$. The computational parameters are the same as in the two computations above. The object is defined as a periodic spline curve, obtained by interpolation through a few specified points.
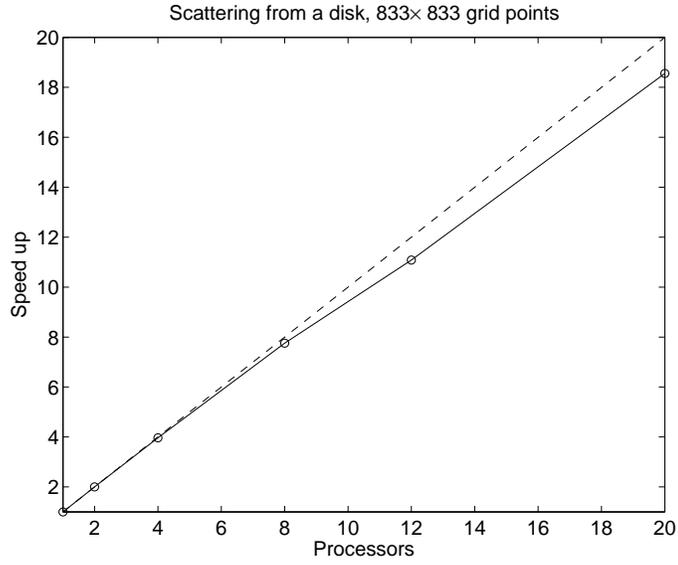
30

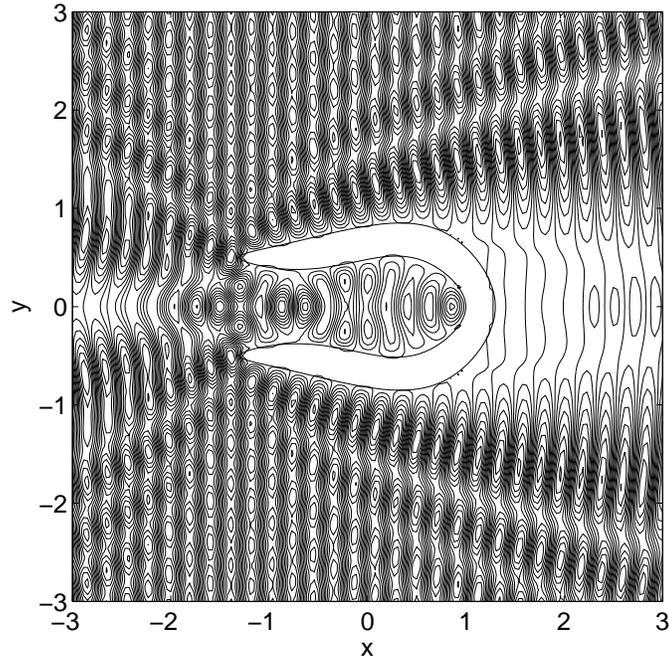Figure 17: Speed-up vs. number of processors. Fixed problem size.

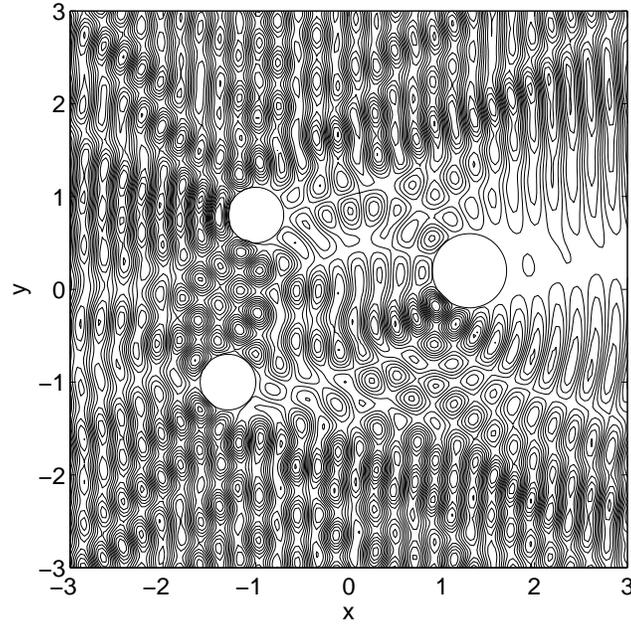Figure 18: $E^{(z)}$ contour lines, horseshoe geometry.

31

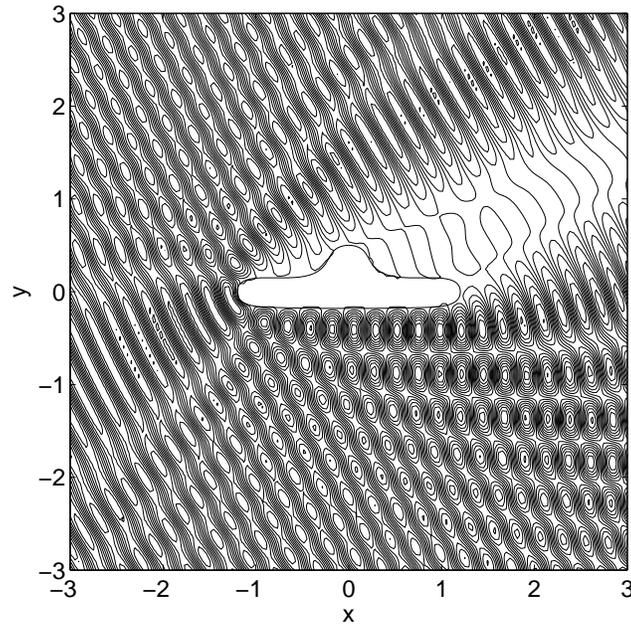Figure 19: $E^{(z)}$ contour lines, multiple cylinders.

Figure 20: $E^{(z)}$ contour lines, unidentified object.

32

6   Conclusions

We have presented a second order accurate scheme for the two-dimensional Maxwell's equations in domains external to perfectly conducting objects of complex shape. The equations are discretized using a node-centered finite-difference scheme on a Cartesian grid and the boundary condition are discretized to second order accuracy employing an embedded technique which does *not* suffer from a "small-cell" time-step restriction in the explicit time-integration method. The computational domain is truncated by a PML. We have derived estimates for both the error due to reflections at the outer boundary of the PML, and due to discretizing the continuous PML equations. Using these estimates, we have shown how the parameters of the PML can be chosen to make the discrete solution of the PML equations converge to the solution of Maxwell's equations on the unbounded domain, as the grid size goes to zero.

We are interested in extending the method to treat discontinuous wave propagation speeds, where the discontinuity extends into the PML. We also plan to extend the method to the three-dimensional Maxwell's equations in external domains.

References

[1] S. Abarbanel, D. Gottlieb, and J. S. Hesthaven, *Long time behavior of the perfectly matched layer equations in computational electromagnetics*, J. Sci. Comput., 17 (2002), pp. 405–422.

[2] B. Alpert, L. Greengard, and T. Hagstrom, *Rapid evaluation of nonreflecting boundary kernels for time-domain wave propagation*, SIAM J. Numer. Anal., 37 (2000), pp. 1138–1164.

[3] S. Asvadurov, V. Druskin, M. N. Guddati, and L. Knizhnerman, *On optimal finite-difference approximations of PML*, SIAM J. Numer. Anal., 41 (2003), pp. 287–305.

[4] C. A. Balanis, *Advanced Engineering Electromagnetics*, Wiley, New York, 1989.

[5] J. P. Berenger, *A perfectly matched layer for the absorption of electromagnetic waves*, J. Comput. Phys., 114 (1994), pp. 185–200.

[6] F. Collino and P. Monk, *The perfectly matched layer in curvilinear coordinates*, SIAM J. Sci. Comput., 19 (1998), pp. 2061–2090.

[7] T. A. Driscoll and B. Fornberg, *Block pseudospectral methods for Maxwell's equations II: Two-dimensional, discontinuous coefficient case*, SIAM J. Sci. Comput., 21 (1999), pp. 1146–1167.

[8] B. Engquist and A. Majda, *Radiation boundary conditions for acoustic and elastic wave calculations*, Comm. Pure. Appl. Math., 32 (1979), pp. 313–357.

[9] D. Givoli and B. Neta, *High-order non-reflecting boundary scheme for time-dependent waves*, J. Comput. Phys., 186 (2003), pp. 24–46.

[10] R. L. Higdon, *Absorbing boundary conditions for difference approximations of the multi-dimensional wave equation*, Math. Comput., 47 (1986), pp. 437–459.

[11] J. S. Juntunen, N. V. Kantartzis, and T. D. Tsiboukis, *Zero reflection coefficient in discretized PML*, IEEE Microwave Wireless Components lett., 11 (2001), pp. 155–157.

[12] H.-O. Kreiss and J. Lorenz, *Initial-Boundary Value Problems and the Navier-Stokes Equations*, Academic Press, 1989.

[13] H.-O. Kreiss and N. A. Petersson, *A second order accurate embedded boundary method for the wave equation with Dirichlet data*, UCRL-JRNL 202686, Lawrence Livermore National Lab, 2004. (submitted to SIAM J. Sci. Comput.).

[14] H.-O. Kreiss, N. A. Petersson, and J. Yström, *Difference approximations for the second order wave equation*, SIAM J. Numer. Anal., 40 (2002), pp. 1940–1967.

[15] ——, *Difference approximations of the Neumann problem for the second order wave equation*, UCRL-JC 153184, Lawrence Livermore National Lab, 2003. (to appear in SIAM J. Numer. Anal.).

[16] P. G. Petropoulos, *Reflectionless sponge layers as absorbing boundary conditions for the numerical solution of Maxwell equations in rectangular, cylindrical, and spherical coordinates*, SIAM J. Appl. Math., 60 (2000), pp. 1037–1058.

[17] ——, *Reflectionless sponge layers for the numerical solution of Maxwell's equations in cylindrical and spherical coordinates*, Appl. Numer. Math., 33 (2000), pp. 517–524.

[18] A. Taflove and S. C. Hagness, *Computational Electrodynamics*, Artech House Publishers, second ed., 2000.

[19] Z. Wu and J. Fang, *High-performance PML algorithms*, IEEE Microwave Guided Wave Lett., 6 (1996), pp. 335–337.

University of California
Lawrence Livermore National Laboratory
Technical Information Department
Livermore, CA 94551